

Suppression of two-dimensional vortex-induced vibration with active velocity feedback controller

B Ma and N Srinil*

School of Marine Science and Technology, Newcastle University, Armstrong Building, Newcastle upon Tyne, NE1 7RU, United Kingdom

*Corresponding author: narakorn.srinil@newcastle.ac.uk

Abstract. Vortex-induced vibrations (VIV) establish key design parameters for offshore and subsea structures subject to current flows. Understanding and predicting VIV phenomena have been improved in recent years. Further, there is a need to determine how to effectively and economically mitigate VIV effects. In this study, linear and nonlinear velocity feedback controllers are applied to actively suppress the combined cross-flow and in-line VIV of an elastically-mounted rigid circular cylinder. The strongly coupled fluid-structure interactions are numerically modelled and investigated using a calibrated reduced-order wake oscillator derived from the vortex strength concept. The importance of structural geometrical nonlinearities is studied which highlights the model ability in matching experimental results. The effectiveness of linear vs nonlinear controllers are analysed with regard to the control direction, gain and power. Parametric studies are carried out which allow us to choose the linear vs nonlinear control, depending on the target controlled amplitudes and associated power requirements.

1. Introduction

Controlling or suppressing VIV has drawn a considerable attention over years for economical and technical interests in enhancing safety, efficient operation and life time of the offshore structures. A wide range of control methods have been proposed and attempted. The methods can generally be categorized into active and passive controls. Passive controls such as employing strakes, shrouds and tripping wires have been investigated over past decades [1, 2]. Different from passive controls, an active control aims to suppress vibrations by inputting external energy source into either the flow or the structure through actuators possessing better flexibility [3].

The active flow control is widely utilized for suppression of the vortex shedding process. Chen and Xin [4] experimentally investigated the controlling effectiveness of the suction flow rate on VIV and they found an optimal solution for suppressing maximum responses. Likewise, Muralidharan and Muddada [5] modelled a blowing and two suction slots positioned on the cylinder and studied the controlling effects from them numerically. They found a good control ability from the control system when the actuations were three times of the free stream. Besides, some other typical control strategies such as acoustic actuations [6] and rotational cylinders [7] have been investigated.

In addition to flow control, a more straightforward approach is to suppress VIV through controlling motion of the cylinder directly. Baz and Ro [8] experimentally investigated the influence of a velocity feedback controller on one-degree-of-freedom (1-DOF) VIV which can generate an adversely



proportional signal to the cylinder velocity. The control action on the cylinder is achieved by an electromagnetic actuator. From the results, it is found that VIV responses are attenuated by more than 80% in the synchronization region. Meanwhile, the experimental results were validated by comparing with theoretical results obtained from a wake oscillator model, which is based on a modified van der pol equation and analytically solved with a motion equation containing control force in a coupled manner via steady state solutions. By tuning three empirical parameters to match experimental observations, theoretical predictions were found to show agreement with controlled and uncontrolled experimental results especially over the synchronization region.

A velocity feedback control for a high mass ratio fluid-structure system was also studied by Mehmood and Abdelkefi [9], where linear and nonlinear active feedback controllers for transverse VIV oscillations were investigated numerically through CFD. Both controllers are functional in reducing VIV in the lock-in range. Suppression of high-amplitude oscillations and the optimal law for desired controlled amplitudes were studied through power comparison between linear and nonlinear manners. In addition to experiments and CFD, the VIV-controller was also applied associated with a wake oscillator by Dai and Abdelkefi [10]. A time-delay feedback controller was modelled in the motion equation to study suppression performance on VIV. The controlling system was solved numerically with a van der pol oscillator in the cross-flow direction. A linear analysis was conducted regarding the effects from various control gains and time-delayed terms on the coupled damping and frequency by ignoring fluid forces and associated nonlinear terms. Then, the influence from the controller on responses of the nonlinear coupled system was determined. They found that choosing controller parameters properly led to effective reductions on VIV. Warui and Fujisawa [11] proposed a velocity feedback controller, where feedback signals can be detected by hot wires and fed back to an actuator. The results demonstrated attenuation of the vortex shedding and the vortex formation process was visualized through a smoke wire method.

Problems based on both line-in and cross-flow directions start to be a key concern since in-line VIV influences on cross-flow VIV in a coupled manner. Hasheminejad and Rabiee [12] investigated an adaptive fuzzy sliding mode controller on 2-DOF VIV. The simulation results indicated a great performance of suppressing both in-line and cross-flow VIV. Besides, the control action was observed to have influence on the vortex shedding process and the vortex formation.

The above literature review implies that, even though the active control of VIV regarding elastically mounted cylinder has been explored in different flow regimes by various methods both numerically and experimentally, the investigation on VIV-controller for strongly coupled 2-DOF fluid-structure interaction problems is still rather limited. Therefore, in this paper, we focus on the control strategies for 2-DOF VIV of a circular cylinder in sub-critical flow regime with a relatively low mass ratio, which is practical for offshore applications. Two types of active feedback controllers are modelled associated with newly developed Duffing-vortex wake oscillators, imparting a control force proportional to single and cubic velocity of the cylinder. The oscillator employed is a reduced-order model including two dimensional motion equations with geometrical nonlinearities and only one wake oscillator. The vortex oscillator is derived from the vortex strength concept, whereby the two dimensional fluid forces are modelled through the displacement of vortex circulation [13].

The model is calibrated and validated through comparing with experimental data in previous literature. Comparisons of different control strategies such as the implement position of controller and the effectiveness of linear and nonlinear controllers are carried out for determining the optimal control law. The present study not only sheds some lights on active feedback design and operation but also serves as a robust prediction model for further experimental investigation.

2. Modelling of controlled fluid-structure interaction system

An elastically supported circular cylinder is concerned and represented by a mass-damper-spring system shown in figure 1. The dynamic system is subjected to a uniform flow and allowed to move in 2-DOF inline and transverse directions. An active controller (linear or nonlinear) is installed on the cylinder and it can be arranged in either X or Y direction. The function of linear/nonlinear controllers is to impart a

force proportional to the cylinder velocity. It is also worth mentioning that the mass and spring stiffness in in-line and cross-flow directions are assumed to be exactly the same and thus the structural governing equations can be expressed as:

$$(m_s + m_a)\ddot{X} + (c_s + c_f)\dot{X} + K_x(X + \alpha_x^* X^3 + \beta_x^* XY^2) = F_x(t) - F_{xc}, \quad (1)$$

$$(m_s + m_a)\ddot{Y} + (c_s + c_f)\dot{Y} + K_y(Y + \alpha_y^* Y^3 + \beta_y^* Y X^2) = F_y(t) - F_{yc}. \quad (2)$$

For linear control,

$$F_{xc} = K\dot{X}, \quad F_{yc} = K\dot{Y}. \quad (3)$$

For nonlinear control,

$$F_{\text{xc}} = G\dot{X}^3, \quad F_{\text{yc}} = G\dot{Y}^3, \quad (4)$$

where X and Y represent inline and transverse cylinder displacements, respectively. Overdots denote the differentiation with respect to the dimensional time t . m_s is the structural mass, m_a the fluid added mass expressed as $m_a = \frac{C_a \pi D^2 \rho}{4}$ where C_a is the added mass coefficient assumed to be unity for a circular cylinder [14], ρ the fluid density, D the cylinder diameter. c_s and c_f are the structural and the fluid added damping, respectively. K_x (K_y) defines the stiffness coefficient in the in-line (cross-flow) direction. The linear or nonlinear control force can be arranged into either direction (F_{xc} or F_{yc}) for which K and G are positive constants characterizing linear and nonlinear control gains, respectively.

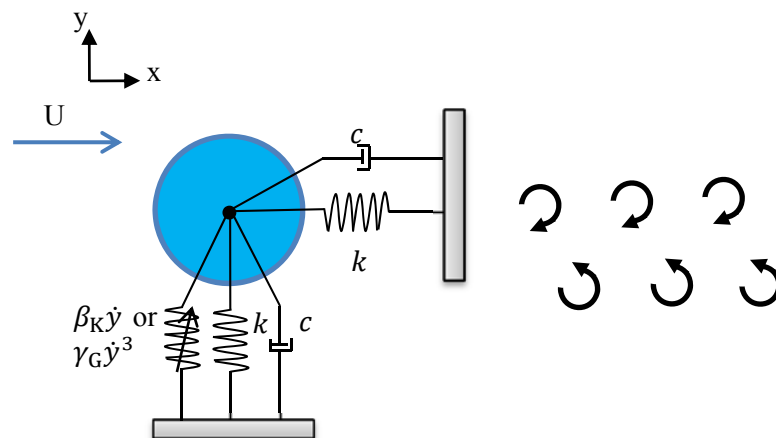


Figure 1. A schematic model of an elastically mounted circular cylinder undergoing 2-DOF VIV and with an active velocity feedback controller

It is well known that typical VIV models often employ a linear structural oscillator to describe cylinder responses [15] whereas the present model takes geometric nonlinearities into account to define stretching effects (X^3, Y^3) and two dimensional x - y coupled motions (XY^2, YX^2) [16]. ($\alpha_x^*, \beta_x^*, \alpha_y^*, \beta_y^*$) are geometrically nonlinear parameters. With introducing the dimensionless time $\tau = t\omega_{st}$, in which ω_{st} is the vortex shedding frequency in rad/s, the reduced displacements are $x = X/D$ and $y = Y/D$. The 2-DOF system modelled by two coupled equations can be expressed in non-dimensional formats as:

$$\ddot{x} + \left(2\xi\delta + \frac{\gamma}{\mu}\right)\dot{x} + \delta^2(x + \alpha_x x^3 + \beta_x xy^2) = -\alpha_{x1} \frac{\pi St}{2\mu} \dot{q}\ddot{q} - F_{xc}^*, \quad (5)$$

$$\ddot{y} + \left(2\xi\delta + \frac{\gamma}{\mu}\right)\dot{y} + \delta^2(y + \alpha_y y^3 + \beta_y y x^2) = \alpha_{y1} \frac{1}{2\pi s_{tu}} \dot{q} - F_{yc}^*. \quad (6)$$

For linear control,

$$F_{xc}^* = \beta_K \dot{x}, \quad F_{yc}^* = \beta_K \dot{y}. \quad (7)$$

For nonlinear control,

$$F_{xc}^* = \gamma_G \dot{x}^3, \quad F_{yc}^* = \gamma_G \dot{y}^3, \quad (8)$$

where $\delta = \frac{\omega_n}{\omega_{st}}$ is the reduced angular structural frequency [15], $\xi = \frac{c_s}{(2m\omega_n)}$ the structural damping coefficient, m the total mass, ω_n the angular structural natural frequency, γ the stall parameter assumed to be 0.5 and related to the mean drag coefficient [17]. $\mu = \frac{m}{\rho D^2}$ is noted as the mass ratio coefficient [15]. $(\alpha_{x1}, \alpha_{y1})$ are empirical parameters associated with drag and lift coefficients (C_{D0}, C_{L0}) of a stationary cylinder and can be expressed as $\alpha_{x1} = \frac{C_{D0}}{8\pi^3 St^3}$ and $\alpha_{y1} = \frac{C_{L0}}{8\pi St}$, where St is the Strouhal number assumed to be 0.19 in the sub-critical flow range of Reynolds number (Re), $C_{D0} = 0.2$ [18] and $C_{L0} = 0.3$ [17]. $(\alpha_x, \beta_x, \alpha_y, \beta_y)$ are the non-dimensional geometric parameters characterizing structural nonlinearities. $\beta_K = \frac{K_c}{m\omega_{st}}$ and $\gamma_G = \frac{GD^2\omega_{st}}{m}$ define dimensionless linear and nonlinear gains, respectively.

A single reduced-order wake oscillator is employed rather than the typical two oscillators reported in many literature [16, 19]. The wake oscillator is derived from the vortex strength concept and can be functional for 2-DOF VIV problems. By introducing the dimensionless displacement of vortex circulation $q(t)$, the vortex strength wake oscillator can be expressed in dimensionless form as [13]:

$$\ddot{q} - \varepsilon(1 - \lambda \dot{q}^2)\dot{q} + q = \beta \dot{y}. \quad (9)$$

(ε, β) are empirical parameters and λ is determined by Re and cross-flow displacement response of the structure, assumed to be 0.2 in the present model. It is noted that the vortex strength wake oscillator is different from the one applied by Facchinetti et al. [15], where the van der pol viscous term $\varepsilon(1 - \dot{q}^2)\dot{q}$ and the acceleration coupling term $\beta \ddot{y}$ are employed. However, the present model utilizes a nonlinear damping term referring to the Rayleigh equation [20] and a velocity coupling term $\beta \dot{y}$. More detailed interpretation of the wake oscillator can be found in the work done by Bai and Qin [13].

Table 1. Empirical parameters for upper and lower branches of cylinder with different m^*

m^*	ε_U	β_U	ε_L	β_L
2.6	0.058	12	1	20
6.9	0.12	12	1	20

3. Validation

The validation is carried out by comparing results obtained from the present model with experimental results [21], where a 2-DOF dynamic system is allowed to move in in-line and crossflow directions. Two different sets of mass-damping values ($m^* = 2.6, \xi = 0.00361$ and $m^* = 6.9, \xi = 0.00145$) are considered with equivalent mass ratios (m^*) and structural natural frequencies (f_n). In this case, the mass ratio (m_{y^*}) and natural frequency (f_{ny}) of the cross-flow direction are precisely the same as the in-line mass ratio (m_{x^*}) and natural frequency (f_{nx}), respectively. Re within the sub-critical flow regime is concerned and the reduced velocity $V_r = \frac{U}{f_n D}$ is up to 14. We firstly perform the numerical simulations by utilizing a 4th order Runge-Kutta method without the control law (i.e. $\beta_K = \gamma_G = 0$). Two dimensionless structural oscillators and one vortex strength oscillator equation (as in equation (5), (6) and (9)) are integrated in time domain simultaneously in a coupled manner with initial conditions of $x = y = \dot{x} = \dot{y} = \dot{q} = 0$ and $q = 2$. Empirical parameters $\varepsilon_U, \varepsilon_L$ and β_U, β_L are tuned by fitting experimental results; they are summarized in Table 1 for each considered m^* , where the subscripts U

and L represent upper and lower branches, respectively. $(\alpha_x, \beta_x, \alpha_y, \beta_y)$ are assumed to be 0.4 initially. The simulation is carried out with 500 time steps which are sufficient for the coupled system to reach a steady state. Also, dynamic response time histories are analysed by the Fast Fourier Transform (FFT) to capture oscillation frequencies (f_o).

Oscillation amplitudes ($\frac{A_x}{D}$ and $\frac{A_y}{D}$) are considered with respect to $m^* = 2.6$ and 6.9. Meanwhile, in order to address the effects from nonlinear terms in equation (5) and (6), response amplitudes simulated from the present model are demonstrated with and without geometric nonlinearities. It is normally reported in the literature that one set of empirical parameters is utilized to describe the dominant upper branch [13, 16], while the occurrence of a lower branch is also evident especially at relatively low m^* [21]. In this study, two sets of (ε, β) over the V_r range are applied to capture different response branches: β_U, ε_U are employed from the beginning of the simulation until reaching the maximum response; β_L, ε_L are then applied right after the occurrence of a response jump from upper branch to lower branch.

Figure 2 indicates the variation of numerical and experimental VIV responses according to different reduced velocities up to $V_r = 14$. Results in cross-flow and in-line directions from the high m^* case are demonstrated in figure 2a and c, respectively. It is observed that there are no significant differences between the amplitudes based on the linear (circles) and nonlinear (triangles) models, where both of the two models are able to capture jumps at onsets of lock-in and lock-out (around $V_r = 4$ and $V_r = 8$, respectively). In addition, numerical results based on linear and nonlinear models are generally in a good agreement with experimental results (solid dots), although in-line responses (figure 2c) are somewhat overestimated. However, when a relatively low m^* is considered (figure 2b and d), the nonlinear terms have obvious effects on the simulation results. The response amplitudes based on the nonlinear model demonstrate a jump down between the upper and lower branches. This is consistent with the experimental responses. In contrast, response amplitudes from the linear model vary without a jump.

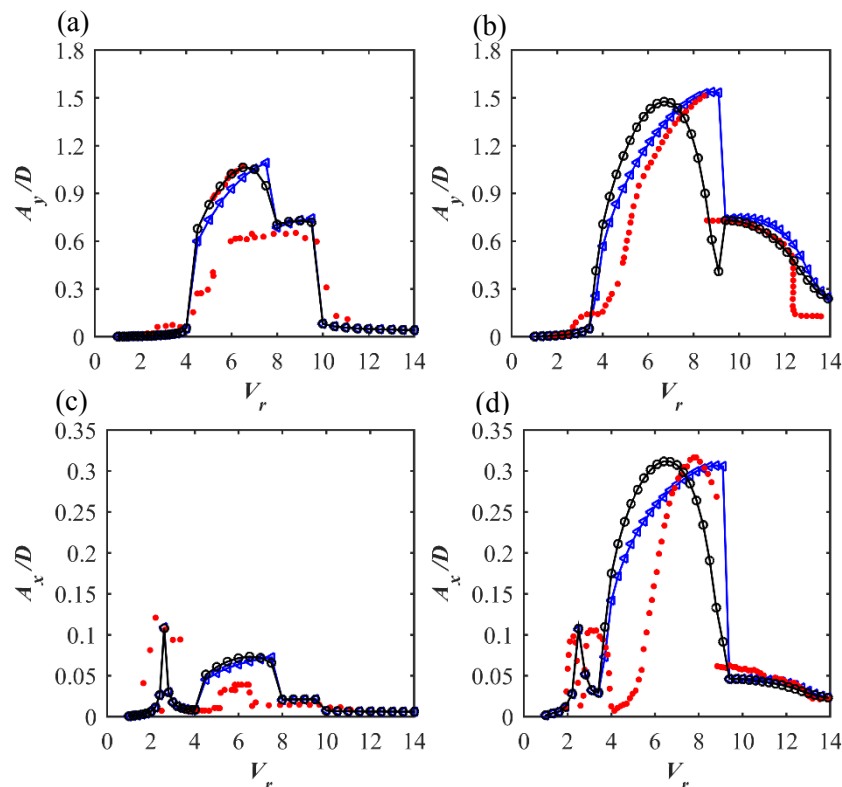


Figure 2. Comparison of response amplitudes between numerical and experimental results: triangles, circles and red dots represent nonlinear, linear and experimental results [21], respectively. (a), (c) and (b), (d) are 2-DOF results based on $m^* = 2.6$ and 6.9, respectively.

Figure 3a and b demonstrate the numerically-obtained frequency ratio (f^*) of f_o to f_n in both directions. For the comparison purpose, cross-flow f^* from the experimental observations [21] are also shown accordingly and denoted as squares. It is noted that cross-flow f^* from two sets of empirical parameters (solid dots in figure 3b) show a better agreement with experimental results than those from the one-set simulation (figure 3a) over the range of lower branch ($8 < V_r < 12$), which again evaluates a better role of the two-set-parameter model in predicting key features of cases with low m^* . Meanwhile, clear 2:1 ratios of in-line (circles) to cross-flow (solid dots) f^* are shown in the results, which demonstrates the ability in capturing the key dual resonances. Besides, it is found that f^* predicted by the current model is not unity over the lock-in region, which means that f_o is not the same as f_n . This is expected and reasonable because the hydrodynamic added mass tends to be variable during VIV, leading to varying f^* over lock-in region [22].

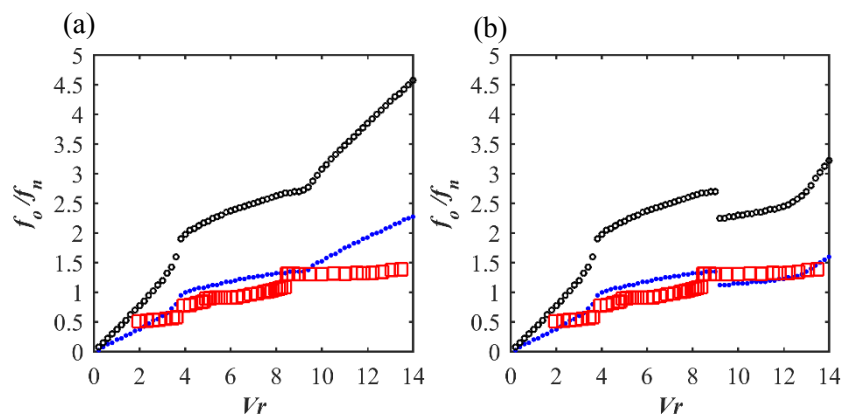


Figure 3. Comparison of f^* between (a) one- and (b) two-set parameter (b) models: circles and solid dots present in-line and cross-flow numerical results; squares present cross-flow experimental results.

4. Results and discussion

4.1. X or Y controller

The controller effectiveness is investigated through a two-set-parameter model based on $m^* = 2.6$ and $\xi = 0.00361$, which has shown a fairly good agreement with experimental observation.

We firstly carry out the numerical simulation of linear and nonlinear active controllers in transverse direction ($F_{xc}^* = 0$ and $F_{yc}^* \neq 0$) with a non-dimensional control gain of $\beta_K = 0.5$. Comparisons between linearly controlled and non-controlled response amplitudes in two directions are shown in figure 4a and c. It is observed that controlled responses (circles with lines) are much lower than non-controlled responses (squares with lines) in the synchronization region. Based on the above comparison, the linear controller is relocated from y to x direction with the same gain ($F_{xc}^* \neq 0$ and $F_{yc}^* = 0$) and it is found that differences between non-controlled amplitudes and controlled amplitudes (lines) are extremely minor even in the lock-in region. This suggests that the in-line controller is not as effective as the cross-flow controller in suppressing VIV responses over the synchronization regime. Similarly, the nonlinear controller is also implemented in transverse and in-line directions with a non-dimensional gain of $\gamma_G = 0.5$ (figure 4b and d). In this case, the cross-flow controller still demonstrates a better effectiveness than the in-line controller. However, the reduced responses are still greater than those with the linear control.

4.2. Control gain effect

Since the Y controller is more effective, simulation in the following discussion is mainly associated with the transverse controller. The effects from the gain on response amplitudes are shown in figure 5 by varying β_K and γ_G from 0 to 0.5 with an increment of 0.1.

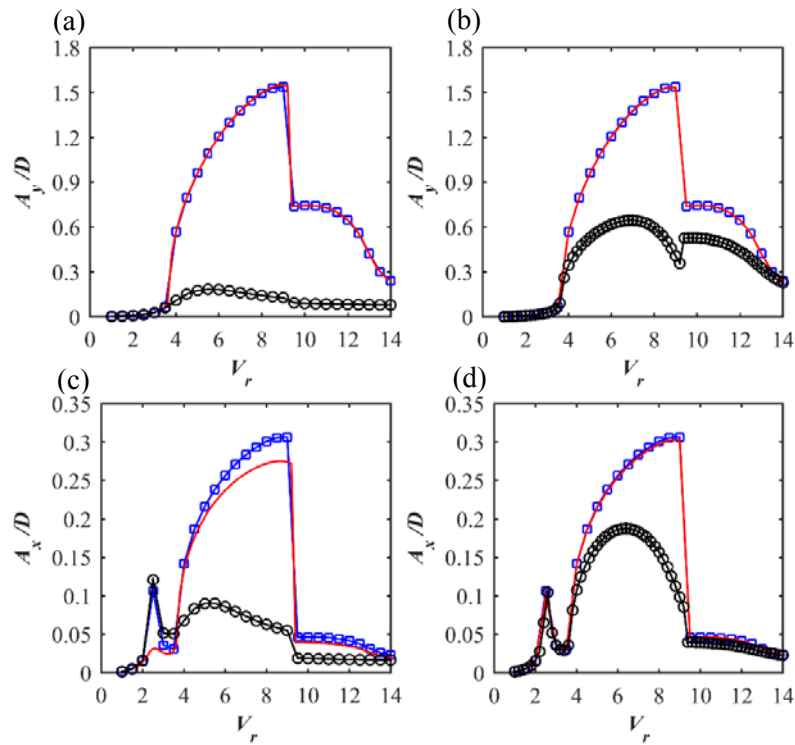


Figure 4. Comparison of controlled vs non-controlled amplitudes: lines, circles and squares represent results from the X controller, Y controller and no-control, respectively. (a) and (c) ((b) and (d)) are 2-DOF results based on linear (nonlinear) control.

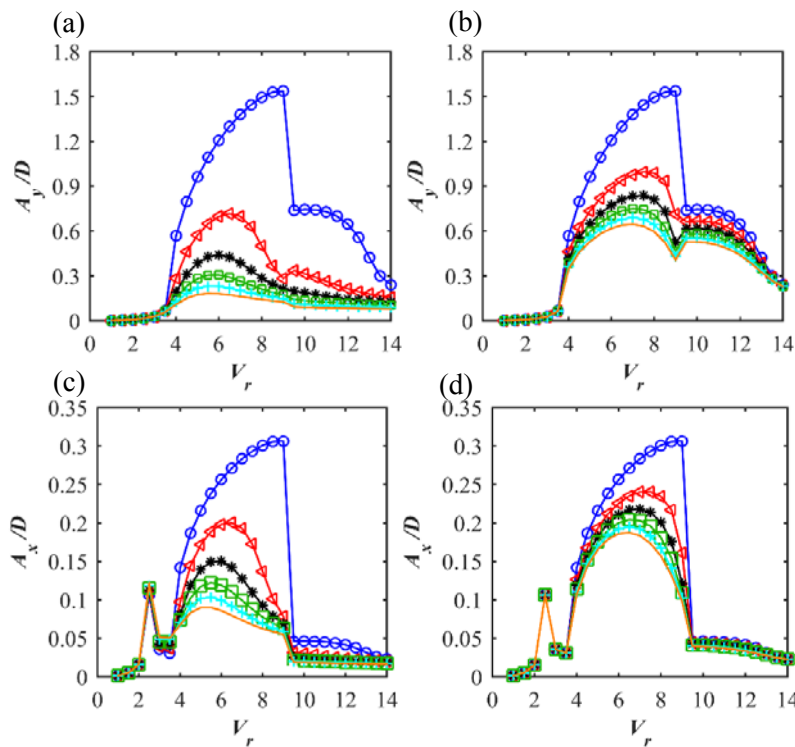


Figure 5. Variation of controlled amplitude responses with V_r : circles, triangles, stars, squares, crosses and lines represent $\beta_K = \gamma_G = 0, 0.1, 0.2, 0.3, 0.4, 0.5$, respectively. (a) and (c) ((b) and (d)) are 2-DOF results based on linear (nonlinear) control.

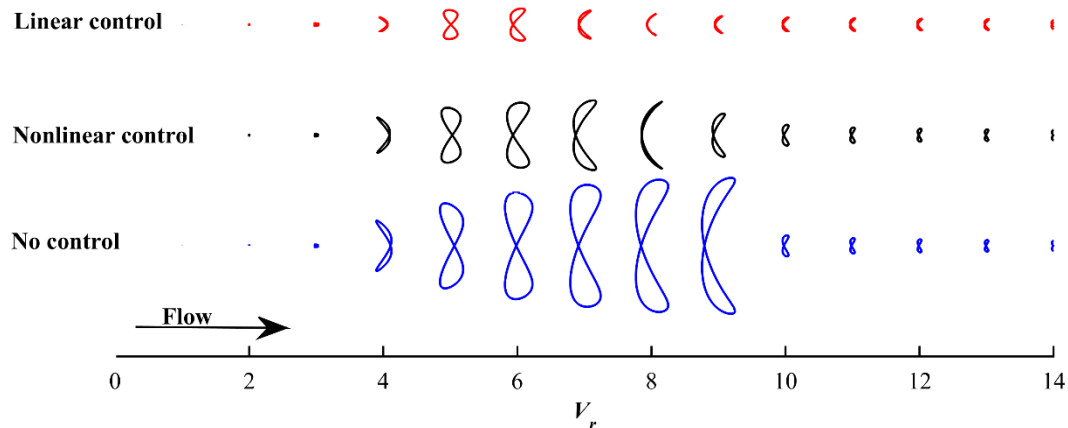


Figure 6. Comparison of non-controlled and controlled ($\beta_K = \gamma_G = 0.25$) x - y trajectories.

For the linear control, it is obvious that amplitudes are reduced gradually with increasing β_K , leading to large reductions up to around 70% and 86% of the in-line and cross-flow VIV, respectively (Figure 5a and c). Likewise, the nonlinear controller also demonstrates the controlling effect on the two dimensional VIV with 41% and 61% amplitude reduction in the x and y directions, respectively (Figure 5b and d). These are not as much as those from the linear controller. Similar qualitative behaviours can be found in the work from [10], where control gains of a time-delay feedback controller based on a 1-DOF wake oscillator model were varied. They observed that as control gains were increased, decreased amplitudes were obtained. It is attributed to a fact that whenever $\beta_K(\gamma_G)$ is risen, the system damping is increased. As a consequence, the whole system behaves in a more damped manner. However, a shift of the lock-in region is not observed; this implies that the oscillation frequency has not been significantly influenced by current controllers. The concept of varying control gains was also employed by Baz A and Ro [8], where a 1-DOF direct velocity feedback control scheme was shown to be able to suppress VIV responses. According to their observation from the experiment, the controller became less effective as the gains increased. This is also demonstrated in our results that the equivalent increase of $\beta_K(\gamma_G)$ leads to less reduced responses.

Linear, nonlinear and non-controlled x - y trajectories with varying V_r are plotted in figure 6, where results represent last ten cycles of steady-state displacements. It is observed that both linear and nonlinear controlled ($\beta_K = \gamma_G = 0.25$) orbital trajectories demonstrate similar figure-of-eight shapes to the non-controlled ones. Thus, we can deduce that the controllers do not affect the tuned 2:1 in-line/cross-flow f^* or appearance of dual resonances. As a further investigation, linear (Figure 7a) and nonlinear (Figure 7b) controlled ($\beta_K = \gamma_G = 0.5$) f^* in two directions are compared with non-controlled results as shown in figure 7. It is seen that in-line (lines) and cross-flow (dashed lines) f^* moderately deviates from non-controlled ones (squares and dots), implying potential effects on VIV vortex shedding process. The larger deviation in figure 7a confirms the more suppressed amplitude by the linear controller. Also, the 2:1 x - y frequency ratios explained the barely changed orbital trajectories in figure 6.

Contour plots regarding control gains and amplitudes are plotted in figure 8 regarding a wide range of V_r which could cover the synchronization region. For the linear controller, it is seen from figure 8a and c that as β_K increases response amplitudes decrease in both two directions. Similar observations are found in nonlinearly controlled amplitudes (figure 8b and d). Apart from the synchronization range, it is interesting to note that the first resonance in the in-line oscillation at around $V_r = 2.5$ is not affected by the controllers (figure 8c and d), remaining the same values with the non-controlled case ($\beta_K = \gamma_G = 0$). Therefore, it should be remarked that Y controller does not affect the in-line first resonance. However, the linear X controller has been observed to be able to suppress the first resonance in figure 4c. This can be explained by the force proportional to in-line velocities imparted by this controller, which deviates the in-line f^* from the unity as shown in figure 3a at $V_r = 2.5$.

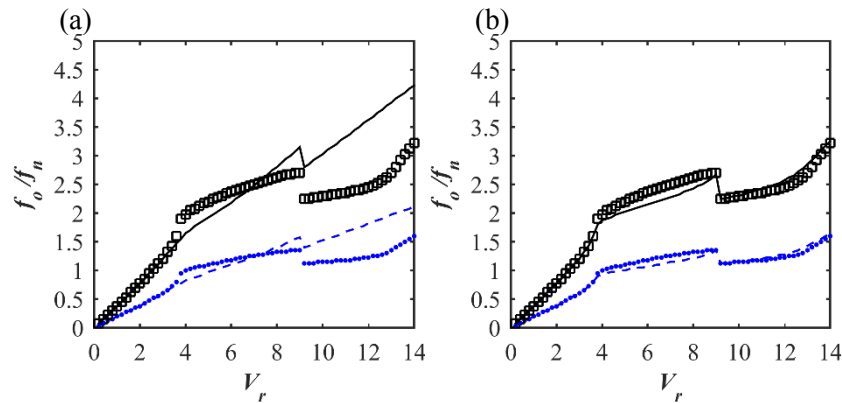


Figure 7. Comparison of f^* with (a) linear and (b) nonlinear controls: line (squares) and dashed lines (dots) represent in-line and cross-flow controlled (non-controlled) results, respectively.

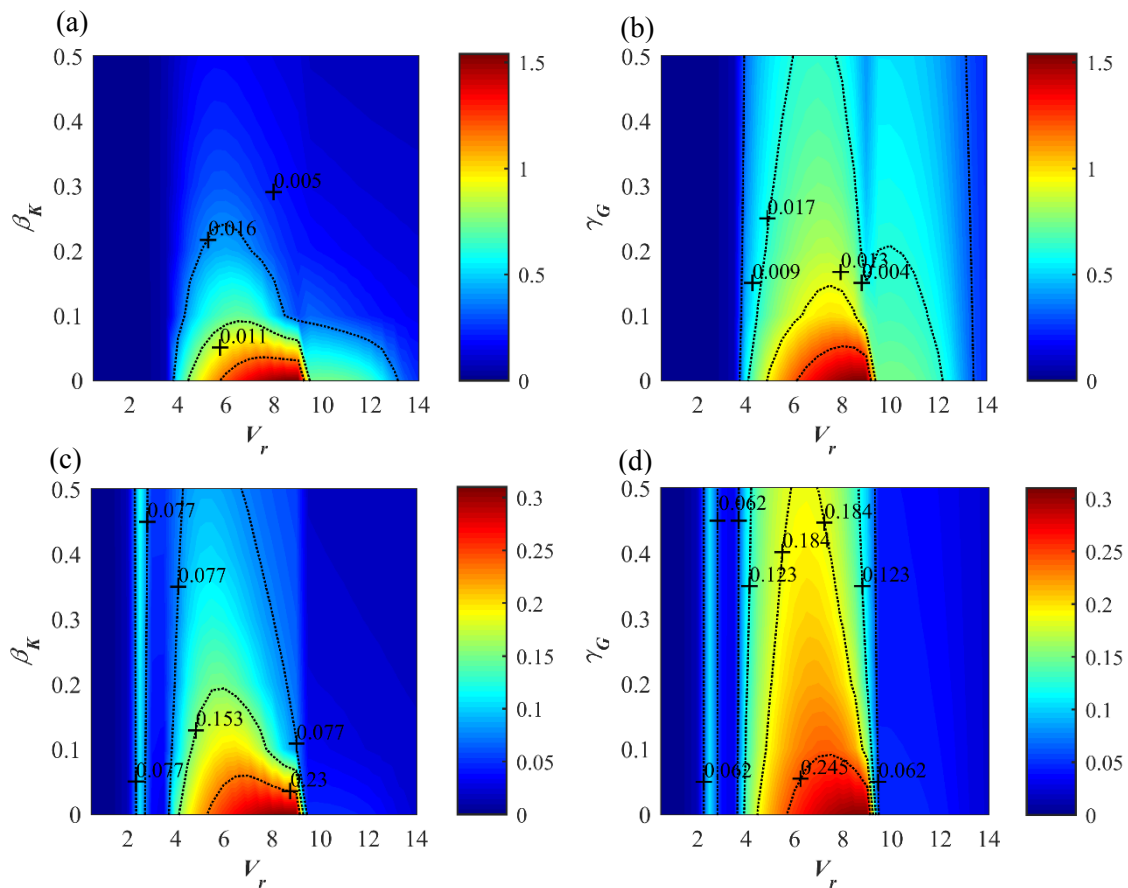


Figure 8. Contour plots of amplitudes with varying β_K (γ_G) and V_r : (a) and (b) are Y amplitudes by linear and nonlinear controls, (c) and (d) are X amplitudes by linear and nonlinear controls, respectively.

4.3. Power comparison

Since the effectiveness is also dependent on forces exerted from controllers, we cannot determine that the linear controller is more effective than the nonlinear one by solely depending on the more reduced amplitudes. Therefore, the control power comparison is introduced.

Figure 9a shows the maximum control power required by the two controllers at $V_r = 7$, where we could observe that the linear controller generally requires lower power than the nonlinear controller.

More specifically, there are no evident differences of maximum power demand between the two controllers when small amount or extremely large reductions are expected. However, when moderate reductions from 30% to 70% are targeted, the linear controller shows advantages of much less power requirements. As the VIV is controlled, it is observed that γ_G tends to be gradually larger than β_K with the same desired amplitude. Plus, values produced by the cubic term are larger than those obtained from the linear term when the desired amplitude is larger than a unity. This is the reason why the nonlinear controller demands increasingly larger power than the linear one up to around $A_y/D = 0.9$. However, when the system is further controlled, the difference between nonlinear and linear control powers becomes smaller. This is because the cubic term from the nonlinear controller starts to generate smaller values than the linear term. Besides, the average power consumption is also considered and comparison between the two controllers at various V_f are shown in figure 9b. In this case, the two suppression strategies demonstrate nearly the same efficiency. Therefore, depending on the maximum power, the linear controller seems to be a better choice. However, when the average power is concerned, both controllers are functional with the same efficiency.

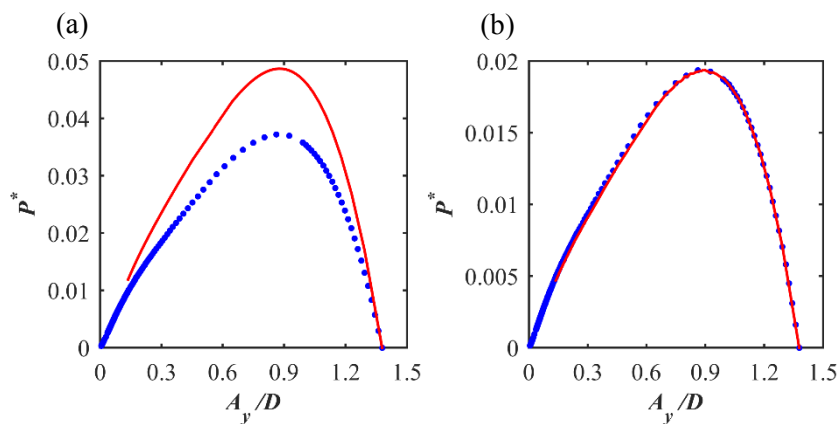


Figure 9. Comparison between linear and nonlinear controllers through (a) maximum and (b) average power consumption: lines (dots) present the power required by nonlinear (linear) controller.

5. Conclusions

Investigations on the effectiveness of linear and nonlinear velocity feedback controllers for 2-DOF VIV of an elastically mounted rigid circular cylinder in uniform flow have been carried out based on the calibrated Duffing-vortex strength wake oscillators. Key VIV characteristics such as lock-in, dual 2:1 resonances and jump phenomena are captured by the present model. Different control strategies are investigated regarding the direction and type of linear vs nonlinear controllers. It is observed that the Y controller is more effective in mitigating 2-DOF VIV than the X controller for the main synchronization regime. On the other hand, the linear X control is functional in reducing the first resonance of in-line oscillations. The effects of control gains on 2-DOF VIV are investigated. Results show that both controllers are able to suppress VIV in both in-line/cross-flow directions, while the control efficiency becomes lessened with higher gains. Similar suppression effects were found in the controllers based on 1-DOF VIV models [8, 10]. Effects on figure-eight trajectories and oscillation frequencies are also studied with varying gains. Both linear and nonlinear controllers fundamentally increase the coupled damping by also changing f^* in in-line and cross flow directions. Nevertheless, the damped system still exhibits the tuned 2:1 of x - y frequency ratios, which can be confirmed by the appearing figure-eight shapes after the control. The optimal control is assessed by comparing maximum and average power demand. According to the comparisons, the two control strategies possess the same efficiency when considering the average power consumption. However, the linear controller – which requires a lower maximum power – shall be chosen when moderate amplitude reductions are expected. Experimental studies are needed to validate theoretical predictions which may be applied to flexible cylinders [23-24].

References

- [1] Wilson J F and Tinsley J C 1989 Vortex Load Reduction: Experiments in Optimal Helical Strake Geometry for Rigid Cylinders *J. Energ. Resour.* **111**(2): p. 72-6.
- [2] Quadrante L A R and Nishi Y 2014 Amplification/suppression of flow-induced motions of an elastically mounted circular cylinder by attaching tripping wires *J. Fluid Struct.* **48**: p. 93–102.
- [3] Inman D J, *Vibration with Control*. 2006: Wiley.
- [4] Chen W, Xin D, Xu F, Li H, Ou J, and Hu H 2013 Suppression of vortex-induced vibration of a circular cylinder using suction-based flow control *J. Fluid Struct.* **42**: p. 25–39.
- [5] Muralidharan K, Muddada S, and Patnaik B S V 2013 Numerical simulation of vortex induced vibrations and its control by suction and blowing *Appl. Math. Modell.* **37**: p. 284–307.
- [6] Fujisawa N and Takeda G 2003 Flow control around a circular cylinder by internal acoustic excitation *J. Fluid Struct.* **17**(7): p. 903-13.
- [7] Filler J R, Marston P L, and Mih W C 1991 Response of the shear layers separating from a circular cylinder to small-amplitude rotational oscillations *J. Fluid Mech.* **231**: p. 481- 99.
- [8] Baz A and Ro J 1991 Active control of flow-induced vibrations of a flexible cylinder using direct velocity feedback *J. Sound Vib.* **146**(1): p. 33–45.
- [9] Mehmood A, Abdelkefi A, Akhtar I, Nayfeh A, Nuhait A, and Hajj 2014 Linear and nonlinear active feedback controls for vortex-induced vibrations of circular cylinders *J. Vib. Control.* **20**(8): p. 1137-47.
- [10] Dai H L, Abdelkefi A, Wang L, and Liu W B 2015 Time-delay feedback controller for amplitude reduction in vortex-induced vibrations *Nonlinear Dyn.* **80**(1-2): p. 59-70.
- [11] Warui H M and Fujisawa N 1996 Feedback control of vortex shedding from a circular cylinder by cross-flow cylinder oscillations *Exp. Fluids.* **21**(1): p. 49-56.
- [12] Hasheminejad S M, Rabiee A H, Jarrahi M, and Markazi A H D 2014 Active vortex-induced vibration control of a circular cylinder at low Reynolds numbers using an adaptive fuzzy sliding mode controller *J. Fluid Struct.* **50**(0): p. 49-65.
- [13] Bai X and Qin W 2014 Using vortex strength wake oscillator in modelling of vortex induced vibrations in two degrees of freedom *Eur. J. Mech. B. Fluids.* **48**: p. 165-73.
- [14] Sarpkaya T 2003 A critical review of the intrinsic nature of vortex induced vibrations *J. Fluid Struct.*
- [15] Facchinetti M L, De Langre E, and Biolley F 2004 Coupling of structure and wake oscillators in vortex-induced vibrations *J. Fluid Struct.* **19**(2): p. 123-40.
- [16] Srinil N and Zanganeh H 2012 Modelling of coupled cross-flow/in-line vortex-induced vibrations using double Duffing and van der Pol oscillators *Ocean Eng.* **53**: p. 83-97.
- [17] Blevins R D, *Flow-induced vibration*. 1990: Van Nostrand Reinhold.
- [18] Currie I and Turnbull D 1987 Streamwise oscillations of cylinders near the critical Reynolds number *J. Fluid Struct.* **1**(2): p. 185-96.
- [19] Dhanwani M A, Sarkar A, and Patnaik B 2013 Lumped parameter models of vortex induced vibration with application to the design of aquatic energy harvester *J. Fluid Struct.* **43**: p. 302-24.
- [20] Hartlen R T and Currie I G 1970 Lift-oscillator model of vortex-induced vibration *J. Eng. Mech. Div.* **96**(5): p. 577-91.
- [21] Jauvtis N and Williamson C 2004 The effect of two degrees of freedom on vortex-induced vibration at low mass and damping *J. Fluid Mech.* **509**: p. 23-62.
- [22] Sumer B M, *Hydrodynamics around cylindrical structures*. 2006: World Scientific.
- [23] Srinil N 2010 Multi-mode interactions in vortex-induced vibrations of flexible curved/straight structures with geometric nonlinearities *J. Fluid Struct.* **26**: p. 1098-1122.
- [24] Srinil N 2011 Analysis and prediction of vortex-induced vibrations of variable-tension vertical risers in linearly sheared currents *App. Ocean Res.* **33**, p. 41-53.